Geophysical Research Letters

RESEARCH LETTER
10.1029/2019GL086438

Magnetopause Compressibility at Saturn with Internal Drivers

Flavien Hardy[1,2], **Nicholas Achilleos**[1,2], **and Patrick Guio**[1,2]

[1]Department of Physics and Astronomy, University College London, London, UK, [2]Centre for Planetary Sciences at UCL/Birkbeck, London, UK

Key Points:
- A data set of magnetopause crossings from the Cassini mission is used to estimate the compressibility of Saturn's magnetosphere
- The method uses a physics-based model of the magnetopause and accounts for variations in system size and internal plasma activity
- The concept of magnetopause compressibility is generalized to account for its response to changes in magnetopause position

Supporting Information:
- Supporting Information S1
- Figure S1

Correspondence to:
F. Hardy,
flavien.hardy.17@ucl.ac.uk

Citation:
Hardy, F., Achilleos, N., & Guio, P. (2020). Magnetopause compressibility at saturn with internal drivers. *Geophysical Research Letters*, *47*, e2019GL086438. https://doi.org/10.1029/2019GL086438

Received 28 NOV 2019
Accepted 3 MAY 2020
Accepted article online 7 MAY 2020

Abstract We use magnetopause crossings of the Cassini spacecraft to study the response of Saturn's magnetosphere to changes in external and internal drivers. We explain how solar wind pressure can be corrected to account for the local variability in internal plasma particle pressure. The physics-based method is applied to perform the most robust estimation of magnetopause compressibility at Saturn to date, using 7 years' worth of magnetometer data from the Cassini mission and accounting for variable internal drivers—particle pressure and azimuthal ring current. The concept of magnetopause compressibility is generalized to quantitatively account for its detailed variation with respect to the position of the magnetopause. An analytical fit is provided to map the compressibility index to values of the stand-off distance. In particular, the procedure shows that the Kronian system appears to behave similarly to that of Jupiter when expanded outwards and more like the Earth's magnetopause when compressed.

1. Introduction

The boundary separating the internal magnetospheric plasma around a magnetized planet from the external solar wind plasma within the magnetosheath, known as the magnetopause, has been shown to be a highly dynamic system (Escoubet et al., 2013; Kaufmann & Konradi, 1969; Masters et al., 2011). Its shape and position are the results of complex interactions between external influences (e.g., incident solar wind, Interplanetary Magnetic Field) and internal drivers leading to an outward pressure (e.g., magnetospheric magnetic field and plasma population). At the gas giants, the total magnetic field has a "disk-like" structure (Achilleos et al., 2010; Arridge et al., 2008; Connerney et al., 1981) due to the magnetic contribution of an extensive equatorial ring current fed internally by moon ejecta (Bagenal & Delamere, 2011; Dougherty et al., 2006; Jia et al., 2010; Kellett et al., 2010; Khurana et al., 2007; Tokar et al., 2006).

Recent empirical models of the magnetopause at Saturn have shown the dynamical behaviour of its magnetosphere to stand in between the relatively rigid, dipolar case at the Earth and the more elastic, compressible case at Jupiter (Arridge et al., 2006; Kanani et al., 2010; Pilkington et al., 2015; Sorba et al., 2017). Pilkington et al. (2015) have notably illustrated how the internal plasma activity can have a large-scale impact on the position and size of the boundary, and Sorba et al. (2017) used a 2-D force balance magnetodisk model of the field (Achilleos et al., 2010) to show how the behavior of Saturn's magnetosphere seems to tend towards a more rigid configuration in a plasma-depleted regime and towards a more compressible, Jupiter-like case in a plasma-loaded state. The influence of the hot plasma population on magnetospheric compressibility is still, however, not fully understood. Most studies are either purely empirical or model based and only provide an "average" description of magnetospheric behavior over very diverse internal and external conditions.

This study provides a physics-based method to determine the compressibility of the magnetopause that accounts for the variability in magnetospheric plasma activity. Section 3 will explain how values for the stand-off distance and upstream solar wind pressure are estimated from magnetopause crossing data. In section 4, we will explain how the impact of internal drivers can be taken into account in the study of magnetopause compressibility. The method is then applied to estimating the boundary compressibility at Saturn and how it varies with system size in section 5.

2. Pressure Balance Method To Estimate System Size and Solar Wind Pressure

2.1. Magnetopause Boundary Position and Pressure Balance Equation

The size and shape of the magnetopause boundary at the gas giants can be estimated, to first order, by solving the pressure balance between external and internal contributions

$$P_{SW}\cos^2\psi + P_0\sin^2\psi = \frac{B^2}{2\mu_0}(1+\beta), \quad (1)$$

where P_{SW} is the solar wind pressure, ψ denotes the angle between the local normal to the magnetopause and the solar wind flow direction, β is the plasma beta corresponding to the ratio of hot plasma pressure to magnetic pressure, and B is the total magnetic field strength with a magnetodisk structure. In this study, B is modeled using a magnetic dipole—aligned with the planetary rotation axis—and an equatorial CAN (Connerney-Acuña-Ness) disk (Connerney et al., 1981, 1983). P_0 denotes the static thermal pressure in the solar wind—assigned a constant value of 10^{-4} nPa (Slavin et al., 1985)—and the coefficient $\sin^2\psi$ is introduced to avoid a complex flow velocity in the subsolar region (Petrinec & Russell, 1997). It is worth noting that the CAN disk used here to model the magnetodisk structure of the field was primarily chosen for its simplicity. It assumes a $1/r$ radial profile for the ring current density, which has been proven inaccurate by Cassini plasma and field measurements (Sergis et al., 2010). The current field model was still shown to organize the observed crossings fairly well (Hardy et al., 2019), but a more realistic ring current model may be considered in future work.

The numerical solution of equation (1) can be considered as representing an equilibrium magnetopause boundary with shape and dimensions fixed by two of the three following parameters: the solar wind pressure P_{SW}, the plasma β accounting for internal plasma activity, and the magnetopause stand-off distance R_{MP}; the parameters of the modeled equatorial ring currents, the inner and outer radii, the disk half-thickness, and the current parameter $\mu_0 I_0$ depend directly on the system's size (Bunce et al., 2007).

The data set used to study the behavior of the magnetosphere at Saturn consists of 1514 magnetopause crossings of the Cassini spacecraft identified using the on-board magnetometer (MAG) and Electron Spectrometer sensor of the Cassini Plasma Spectrometer (CAPS-ELS) instrument, from October 2004 to February 2013 (Pilkington et al., 2015). The trajectory of the spacecraft during this period was shown to adequately sample the mean position of the boundary, with no bias for extreme magnetospheric configurations (Pilkington et al., 2014). Seasonal distortions of the magnetopause are taken into account using the "general deformation method" (Tsyganenko, 1998): the crossing positions are corrected appropriately to model the response of the boundary and current sheet to a dipole tilt with regard to the solar wind flow, observed at Saturn by Arridge et al. (2008).

Local values for the magnetic field strength B and plasma β were acquired by the spacecraft at each crossing position. In order to determine the corresponding equilibrium solar wind pressure P_{SW}, it is necessary to have access to the local geometry of the boundary, as it fixes the angle ψ in equation (1). The morphology of the magnetopause is itself dependent on the system size, since the equatorial ring current–and consequently the magnetodisk structure of the field—responds to how close the surface is to the planet. It is thus necessary to estimate the stand-off distance corresponding to each observed crossing, before trying to determine values of the solar wind pressure.

2.2. Magnetopause Crossings and Magnetospheric Scales

We start by solving the pressure balance equation at Saturn in order to determine a set of equilibrium magnetopause models (Hardy et al., 2019) with integer stand-off distances ranging from 15 to 40 Saturn radii ($R_S \approx 60\,268$ km), each with consistent plasma disk parameters according to the results of Bunce et al. (2007).

The method used to determine the system size is illustrated in Figure 1, in the special case of a crossing M observed in the noon-midnight meridional plane. In the general case, we determine the intersections—shown in purple—between the crossing direction **OM** and the reference surfaces, shown in blue. A spline function is defined to map these intersections with the matching values for the stand-off distance, shown in green along the Sun-planet line. This function is then used to estimate the system size corresponding to the observed crossing position, and the procedure is repeated throughout the entire data set.

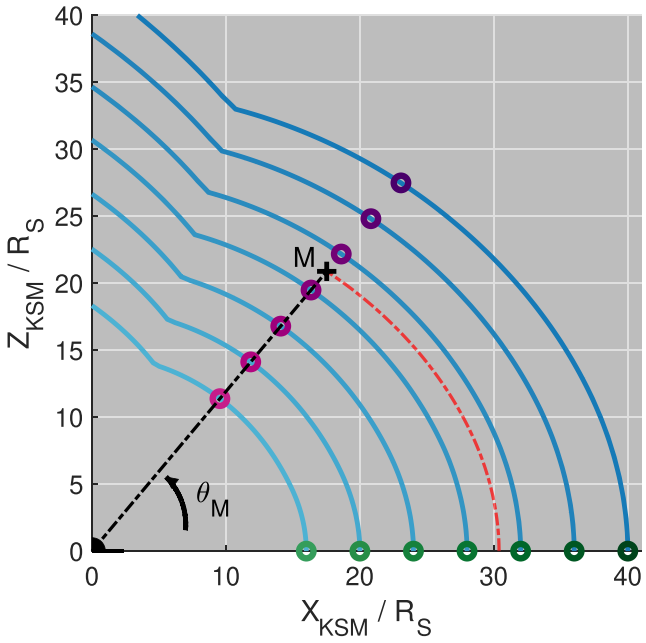

Figure 1. Illustration of the stand-off distance estimation, given a magnetopause crossing M. In purple are the intersections of the crossing direction **OM** with the equilibrium reference surfaces shown in blue; in green are the corresponding positions of the subsolar nose. The red dashed line illustrates the mapping used to determine the system size corresponding to a crossing M. The axes are the ones of the orthogonal, Saturn-centered coordinate system (Kronocentric Solar Magnetospheric frame): X_{KSM} points towards the Sun, and Z_{KSM} is such that the X_{KSM}–Z_{KSM} plane contains Saturn's magnetic dipole. This figure corresponds to the specific case of a crossing observed in the noon-midnight meridional plane ($Y_{KSM} = 0$), but the method is applicable to any crossing position.

2.3. From System Size to Solar Wind Pressure

Now that the equilibrium system size has been determined for each crossing, local values of the solar wind pressure can be estimated. The main difficulty of this step lies in the magnetopause geometry depending on the system's size and us having access to a finite number—rather than a continuum—of equilibrium surfaces. This was addressed through the following procedure: at each crossing M,

- consider the two equilibrium boundaries whose scales are the closest to the stand-off distance estimate;
- these surfaces are used alongside the spacecraft measurements to solve equation (1) at M, resulting in two values for P_{SW};
- the relative position of the subsolar nose with respect to the scales of each reference surface is used to estimate the solar wind pressure at M as a weighted average.

For example, if the stand-off distance corresponding to a crossing M was found to be 22.3 R_S, the reference surfaces of scale 22 R_S and 23 R_S would be used to determine two values for the solar wind pressure, noted $P^*_{SW,\,22}$ and $P^*_{SW,\,23}$, respectively. The solar wind pressure at M would then be estimated as $P_{SW} = 0.7\ P^*_{SW,\,22} + 0.3\ P^*_{SW,\,23}$.

In order to assess the magnetopause compressibility and study the response of the magnetosphere to changes in solar wind pressure, it becomes necessary to account for the variability in local plasma β. Pilkington et al. (2015) used a K-clustering algorithm to group the crossings into three clusters depending on the values of β, with a surface model that includes a 19 % polar flattening (Pilkington et al., 2014). Though this method was able to quantify the impact of internal plasma activity on the stand-off distance, it reduced the number of crossings available to study the boundary compressibility α within each cluster. In particular, the uncertainty in α for the high-β cluster—that is, describing a plasma-loaded magnetosphere—was too high to illustrate any definite impact of plasma activity on magnetopause compressibility. We describe in the following section a method that reduces the number of parameters impacting system size, while accounting for the variability in internal plasma activity over the entire data set.

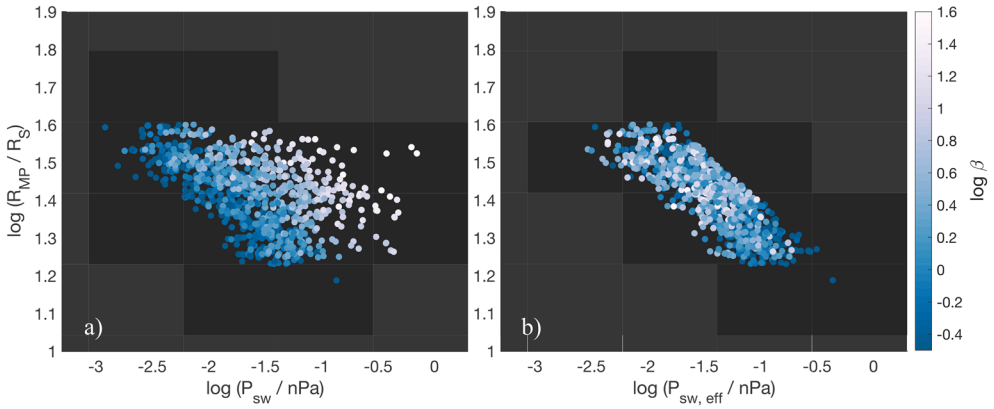

Figure 2. Values for the stand-off distance R_{MP} plotted as a function of (a) the solar wind pressure estimates P_{SW} and (b) the effective solar wind pressure estimates $P_{SW,\,eff}$ introduced in equation (6). The color bar indicates the local values of plasma β. The scaling procedure of section 3.2 eliminates the trend evident in (a), making the values of β much more evenly distributed within the cluster in (b).

3. Compressibility Estimates and Effects of Internal Drivers

3.1. Magnetopause Compressibility and Impact of Internal Particle Pressure

Let R_{MP} and P_{SW} denote the stand-off distance and effective solar wind pressure of a magnetospheric state perturbed by a small change in pressure dP_{SW}. Assuming a regime devoid of magnetospheric plasma, the consequent displacement of the subsolar nose dR_{MP} is assumed to satisfy, to first order,

$$\frac{dR_{MP}}{R_{MP}} \approx -\frac{1}{\alpha}\,\frac{dP_{SW}}{P_{SW}}\,, \tag{2}$$

where α is the compressibility parameter of the boundary; the larger the value of α, the smaller the impact of a change in pressure on system size, and the more "rigid" the magnetopause boundary, and *vice versa*.

Considering infinitesimal changes in pressure, integrating equation (2) leads to the linear relationship

$$\log R_{MP} = -\frac{1}{\alpha}\,\log P_{SW} + \mathrm{cst}\,, \tag{3}$$

or the power law

$$R_{MP} \propto P_{SW}^{-1/\alpha}\,. \tag{4}$$

This expression has been shown to be valid over a wide range of stand-off distance (Achilleos et al., 2008; Bunce et al., 2007), though it is affected by the magnetospheric plasma content. Given a list of crossings with consistent values for the stand-off distance R_{MP} and solar wind pressure P_{SW}, the compressibility parameter α could then be inferred semi-empirically from a linear fit of equation (3). The relationship found between the magnetospheric scales R_{MP} and the solar wind pressure estimates P_{SW} is shown in Figure 2a. The long "trailing off" of the crossings towards the top right of the plane illustrates the broad range in both solar wind pressure and plasma β, which prevents a direct determination of magnetopause compressibility over the entire data set. This trend also shows the large impact of internal plasma activity over magnetospheric scales, consistent with previous observations showing that hot plasma dynamics are competitive with solar wind conditions in determining the system's size (Pilkington et al., 2015). This factor needs to be addressed before performing any fit to the data for determining the value of α.

3.2. Dimensionality Reduction and Plasma β Scaling

Let us start by noticing that the term accounting for the static thermal pressure $P_0\sin^2\psi$ in equation (1) only plays an important role at high-latitude positions, close to the cusp on the dayside at a latitude of $\approx$ 71° (Hardy et al., 2019). Since most of our observed crossings of the Cassini spacecraft occurred at low latitudes around Saturn (with a maximum observed latitude of around 62° and a median latitude of $\approx$ 6°), it is relevant to consider the approximate pressure balance equation

$$P_{SW}\cos^2\psi = \frac{B^2}{2\mu_0}\,(1+\beta)\,. \tag{5}$$

This is equivalent to

$$P_{\mathrm{SW,\,eff}} \quad \cos^2\psi = \frac{B^2}{2\mu_0}\left(1+\beta_{\mathrm{ref}}\right), \tag{6}$$

with β_{ref} denoting a prescribed reference value of plasma beta and $P_{\mathrm{SW,\,eff}} = \frac{P_{\mathrm{SW}}}{(1+\beta)}\left(1+\beta_{\mathrm{ref}}\right)$ an effective, scaled solar wind pressure. Thus, considering the effective pressure $P_{\mathrm{SW,\,eff}}$ in place of the pressure estimates P_{SW} allows us to artificially scale all the crossings to a common reference value of plasma beta β_{ref}. In other words, under the assumption of pressure balance, $P_{\mathrm{SW,\,eff}}$ are the values of the external solar wind pressure that we would expect had all crossings been acquired with the same plasma β.

For $\beta_{\mathrm{ref}} = 3.58$, for example—the mean value of plasma β over the data set—the relationship between the stand-off distance and the effective solar wind pressure is shown in Figure 2b. The color bar seems to indicate that the trend shown in Figure 2a vanishes, and the crossings appear to cluster much closer to each other, as expected. Choosing any other value for β_{ref} would only displace the cluster horizontally, without disrupting the distribution shown in Figure 2b.

3.3. Revisiting the Impact of Internal Plasma Pressure on System Size

Another consequence of scaling the solar wind pressure by considering $P_{\mathrm{SW,\,eff}}$ can be seen in equation (2); it may be expanded as

$$\frac{\mathrm{d}R_{\mathrm{MP}}}{R_{\mathrm{MP}}} \approx -\frac{1}{\alpha}\left(\frac{\mathrm{d}P_{\mathrm{SW,\,eff}}}{P_{\mathrm{SW,\,eff}}}\right) = -\frac{1}{\alpha}\left(\frac{\mathrm{d}P_{\mathrm{SW}}}{P_{\mathrm{SW}}}\right) + \frac{1}{\alpha}\left(\frac{\mathrm{d}\beta}{1+\beta}\right). \tag{7}$$

In the context of the Earth's magnetosphere—which is relatively devoid of plasma at the magnetopause boundary (Shue et al., 1997)—only the first term of the right-hand side of equation (7) contributes to a displacement of the subsolar nose. In this case, the magnetic field can be well approximated by a vacuum dipole and the compressibility index is found to be $\alpha = 6$.

The additional β term necessary for Saturn and Jupiter shows that an enhancement in internal plasma activity acts towards inflating the magnetosphere (note the *plus* sign in front) in such a way that a relative change in β has the same impact as a relative change in P_{SW} if $\beta \gg 1$. This is consistent with the large impact of plasma β on system size illustrated in Figure 2. Additionally, the compressibility parameter is expected to be smaller at the gas giants due to the "disk-like" structure of their magnetic fields: ionized moon ejecta are accelerated towards corotation with the rapidly rotating magnetospheres, harboring an azimuthal ring current that acts towards stretching the field lines radially outwards along the equatorial plane. This would lead to the magnetopause being more compressible when it is expanded (i.e., in a plasma-loaded state) and more similar to the dipole case as it is compressed (i.e., in a plasma-depleted state). This variability of the compressibility with regard to the system size is studied in the following section.

4. System Size and Magnetopause Compressibility

4.1. Filtering Crossings Far From Pressure Balance

In order to estimate how the magnetopause compressibility at Saturn varies depending on the system size, it is necessary to filter out the crossings that were observed while the magnetopause boundary was not close to equilibrium, but strongly accelerating instead.

To do so, at each crossing, the solar wind pressure estimates—derived from the data and the reference surfaces—can be compared with the weighted average of the values corresponding to the equilibrium surfaces of similar scales. Figure 3 shows the crossings that remained after eliminating those for which the aforementioned difference in pressure was larger than 40 % of the corresponding averaged equilibrium values.

Two observations can be made from Figure 3: the crossings appear not to be distributed along a line, but rather along a slightly convex curve instead; this illustrates the impact of system size on magnetopause compressibility. This feature was previously hidden by the variability in plasma β in Figure 2a and drowned by the scatter in Figure 2b; it is studied further in the next subsection. Second, there is an apparent “flaring” in the crossing distribution when moving towards the top left. This could be due to the magnetosphere being less rigid when subjected to changes in solar wind pressure, as the system is expanded: the boundary is then

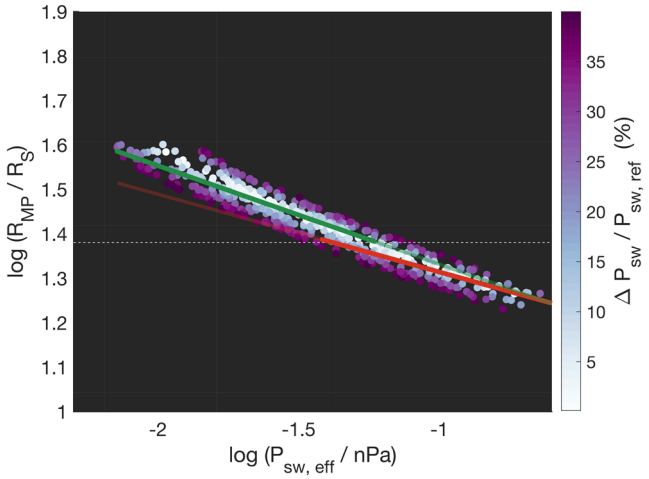

Figure 3. Relationship between the stand-off distance R_{MP} and the effective solar wind pressure estimates $P_{SW,\,eff}$ introduced in equation (6). The color bar indicates the difference in solar wind pressure ΔP_{SW} between the estimated value $P_{SW,\,eff}$ and the reference value from pressure equilibrium $P_{SW,\,ref}$; crossings with a difference smaller than 40 % were kept. The dashed horizontal line indicates $R_{MP} = 24\,R_S$, and the green and orange lines are linear fits of equation (3) to the remaining crossings, for $R_{MP} \geq 24\,R_S$ and $R_{MP} \leq 24\,R_S$, respectively. Considering the entire set of crossings leads to a compressibility $\alpha = 4.17$ and $CI_{95} = [4.08, 4.27]$. However, for $R_{MP} \geq 24\,R_S$, we find $\alpha = 4.51$ with a 95 % confidence interval $CI_{95} = [4.31, 4.72]$; for $R_{MP} \leq 24\,R_S$, we find $\alpha = 5.71$ and $CI_{95} = [5.25, 6.25]$.

more easily pushed away from pressure balance, and a larger number of observed crossing is thus likely to correspond to an accelerating magnetopause.

4.2. Qualitatively Illustrating the Impact of System Size on Magnetopause Compressibility

The impact of system size on magnetopause compressibility can be illustrated by performing two separate linear fits of equation (3) to the crossing distribution shown in Figure 3.

The magnetopause crossings are chosen to be separated into two subsets: one corresponding to an expanded state ($R_{MP} \geq 24\,R_S$) and one corresponding to a compressed state of the magnetosphere ($R_{MP} \leq 24\,R_S$). In the first case, in a plasma-loaded regime (and/or low dynamic pressure regime), the compressibility is found to be $\alpha = 4.51$, with a 95 % confidence interval $CI_{95} = [4.31, 4.72]$; in a plasma-depleted regime (and/or high dynamic pressure regime), as the boundary is pushed closer the planet, $\alpha = 5.71$, with a 95 % confidence interval $CI_{95} = [5.25, 6.25]$ (the statistical interval is given as is, though the compressibility index has a physical upper bound of 6, corresponding to a vacuum dipole case). Such a "bimodal" behavior of the magnetopause is consistent with placing Saturn's magnetosphere in between the Earth's, where $\alpha \approx 6$, and Jupiter's, where $\alpha \approx 4$ (Bagenal & Delamere, 2011). The cut-off value of $24\,R_S$ also echoes with previous observation and modeling studies (Arridge et al., 2011; Sorba et al., 2017) in which a shift in behavior related to magnetic field structure was found around $\approx 22 - 25\,R_S$.

It is worth noting at this stage that the precise position of this "bend" in the crossing distribution—arbitrarily identified here at $R_{MP} = 24\,R_S$—is of little significance. However, it does qualitatively illustrate how the magnetopause compressibility varies with system size and thus motivates further study in its response to changes in the position of the magnetopause.

4.3. Generalizing Magnetopause Compressibility to Account for the Impact of System Size

In the most general case, the response of the system's size R_{MP} to changes in effective solar wind pressure can be described by an equation of the form

$$\log R_{MP} = -\varphi\left(\log P_{SW,\,eff}\right)\ , \tag{8}$$

where R_{MP} denotes the magnetopause stand-off distance, $P_{SW,\,eff}$ the effective solar wind pressure introduced in equation (6), and φ a real function monotonically increasing on the domain considered.

The differentiation of equation (8) leads to

$$\frac{dR_{MP}}{R_{MP}} = -\varphi'\left(\log P_{SW,\,eff}\right)\quad \frac{dP_{SW,\,eff}}{P_{SW,\,eff}}\ . \tag{9}$$

Physically, the coefficient $-\varphi'\left(\log P_{SW,\,eff}\right)$ modulates a relative change in pressure $\frac{dP_{SW,\,eff}}{P_{SW,\,eff}}$ that leads to a relative displacement $\frac{dR_{MP}}{R_{MP}}$ of the magnetopause boundary. The compressibility index α can then be defined as

$$\alpha = \frac{1}{\varphi'\left(\log P_{SW,\,eff}\right)}\ . \tag{10}$$

If the function φ is chosen to be a first-degree polynomial, the relationship described by equation (8) is equivalent to the case of equation (3) with a constant compressibility α. Because we expect α to vary with system size (as shown in Figure 3), it seems necessary to introduce nonlinear terms in the expression of φ.

In the case where φ is defined as a second-degree polynomial

$$\varphi := x \rightarrow a_0 + a_1\,x + a_2\,x^2\ , \tag{11}$$

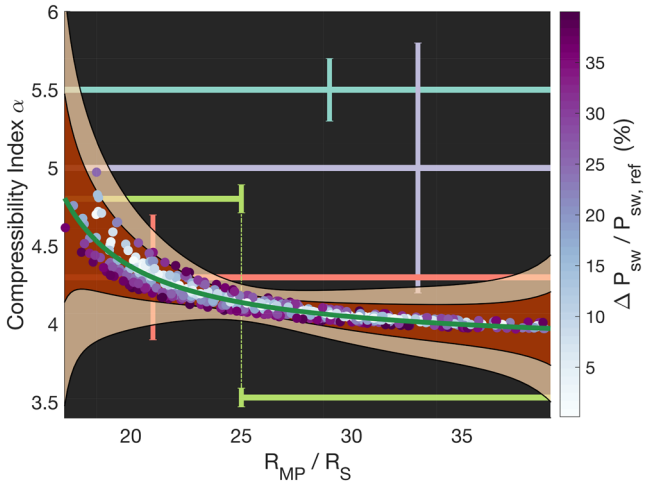

Figure 4. Estimates for the magnetopause compressibility α as a function of system size R_{MP}, for each of the magnetopause crossings shown in Figure 3. The green line represents a hyperbolic fit for α as a function of system size (see section 4.3 and equation 14 for more details). The areas shaded in dark and light orange correspond to the variation in α associated with the 1σ and 2σ confidence bands, respectively. In the background, the values of α determined by Pilkington et al. (2015) (in blue, $\alpha = 5.5 \pm 0.2$), Kanani et al. (2010) (in purple, $\alpha = 5.0 \pm 0.8$), Sorba et al. (2017) (in green, $\alpha(R_{MP} < 25\,R_S) = 4.80 \pm 0.09$, $\alpha(R_{MP} > 25\,R_S) = 3.53 \pm 0.06$), and Arridge et al. (2006) (in red, $\alpha = 4.3 \pm 0.3$) are shown.

equation (10) yields a compressibility of the form

$$\alpha = \frac{1}{a_1 + 2a_2 \log P_{SW,\,eff}}, \tag{12}$$

which hints at a hyperbolic expression for α.

Let us then generalize this idea one step further by considering the parametric expression

$$\alpha = c_0 + \frac{1}{c_1 + c_2 \log P_{SW,\,eff}}, \tag{13}$$

where c_0, c_1 and c_2 are real numbers. The additional parameter c_0 introduces a new degree of freedom in allowing a vertical translation of the hyperbola.

The following procedure can now be performed:

- Using the expression of the compressibility α from equation (13), the integration of equation (10) leads to a functional form for φ.
- A fit of equation (8) to the crossing distribution shown in Figure 3 provides the coefficients in the expression for φ and thus α.
- Using the relationship between the system size R_{MP} and $P_{SW,\,eff}$ shown in Figure 3, α can be plotted with respect to R_{MP}; this is shown in Figure 4.

This final relationship between α and R_{MP} is further described by fitting a hyperbolic expression of the form

$$\alpha(R_{MP}) = a + \frac{1}{b\,R_{MP} - d} \tag{14}$$

to the crossing distribution in Figure 4. The coefficients are found to be $a = 3.83$, $CI_{95} = [3.81, 3.86]$, $b = 3.56$, $CI_{95} = [3.06, 4.06]$, $d = 13.34$, $CI_{95} = [12.74, 13.93]$; this fitted curve is plotted in green in Figure 4. In particular, it is found that $\alpha(R_{MP} = 15\,R_S) = 5.97$ and $\alpha(R_{MP} = 35\,R_S) = 4.00$, which is consistent with the discussion concluding section 4.2. It is worth noting, however, that the uncertainties become relatively large as the system approaches either very compressed or very expanded states; this is mainly due to these extreme states being represented by a relatively small number of observed crossings.

Figure 4 also shows the values of α previously determined by Arridge et al. (2006), Kanani et al. (2010), Pilkington et al. (2015), and Sorba et al. (2017): within the range of stand-off distances observed at Saturn and the uncertainties cited, each of these values intersects the 2σ confidence bands shaded in light orange. In the case of Kanani et al. (2010) and Pilkington et al. (2015), we find that previous considerations of the classic linear relationship of equation (3) may have led to a slight overestimation of the mean magnetopause compressibility. The value and uncertainty for α determined by Arridge et al. (2006) seems to be, on average, in good agreement with our findings. In particular, Sorba et al. (2017) identified a shift in behavior around $25\,R_S$, with two distinct values for the compressibility depending on whether the system is more compressed or expanded: interestingly, the value for α that we find at $25\,R_S$ is very close to the average of the two values determined by the authors. This seems to show that their bimodal modeling approach was able to capture the mean response of the system, though the finer behavioral structure evidenced in Figure 4 was lost. For reference, a comparison of the magnetopause profiles—both in the equatorial and noon-midnight meridional planes—from the aforementioned models is shown in the supporting information.

5. Conclusion

An extensive set of observed magnetopause crossings at Saturn was used to study the response of the planetary magnetosphere to changes in solar wind pressure. Our physics-based three-dimensional magnetopause model that includes an equatorial ring current (dependent on system size) and internal hot plasma particle pressure (with constant plasma β) was used to estimate magnetospheric scales and local values of solar wind pressure, incorporating magnetic and plasma observations from the Cassini spacecraft.

We described how the observed crossings can be scaled to a common value of plasma β in order to account for variable local particle pressure. The compressibility of the magnetopause was studied on two subsets of crossings corresponding to a compressed and expanded system, in order to qualitatively illustrate how the magnetosphere becomes more easily compressible as it expands.

The concept of magnetopause compressibility was further generalized to quantitatively account for its variation with the position of the boundary, and an analytical fit is provided to define it as a function of the stand-off distance. The resulting behavior predicted for compressibility of the system seems to be consistent with the observed variability in magnetic field structure within Saturn's inner and outer magnetosphere and with recent magnetopause modeling studies—both observational and theoretical.

Acknowledgments
FH was supported by a studentship jointly funded by UCL's Perren and Impact schemes. NA and PG were supported by the UK STFC Consolidated Grant (UCL/MSSL Solar and Planetary Physics, ST/N000722/1). The magnetopause crossings of the Cassini spacecraft mentioned in this study were identified by Pilkington et al. (2015) using the Cassini MAG, CAPS-ELS, and MIMI data available from the Planetary Data System (http://pds.nasa.gov/).

References

Achilleos, N., Arridge, C. S., Bertucci, C., Jackman, C. M., Dougherty, M. K., Khurana, K. K., & Russell, C. T. (2008). Large-scale dynamics of Saturn's magnetopause: Observations by Cassini. *Journal of Geophysical Research*, *113*, A11209. https://doi.org/10.1029/2008JA013265

Achilleos, N., Guio, P., & Arridge, C. S. (2010). A model of force balance in Saturn's magnetodisc. *Monthly Notices of the Royal Astronomical Society*, *401*(4), 2349–2371. https://doi.org/10.1111/j.1365-2966.2009.15865.x

Arridge, C. S., Achilleos, N., Dougherty, M. K., Khurana, K. K., & Russell, C. T. (2006). Modeling the size and shape of Saturn's magnetopause with variable dynamic pressure. *Journal of Geophysical Research*, *111*, A11227. https://doi.org/10.1029/2005JA011574

Arridge, C. S., André, N., McAndrews, H. J., Bunce, E. J., Burger, M. H., Hansen, K. C., et al. (2011). Mapping magnetospheric equatorial regions at Saturn from Cassini prime mission observations. *Space Science Reviews*, *164*, 1–83. https://doi.org/10.1007/s11214-011-9850-4

Arridge, C. S., Russell, C. T., Khurana, K. K., Achilleos, N., Cowley, S. W. H., Dougherty, M. K., et al. (2008). Saturn's magnetodisc current sheet. *Journal of Geophysical Research*, *113*, A04214. https://doi.org/10.1029/2007JA012540

Bagenal, F., & Delamere, P. A. (2011). Flow of mass and energy in the magnetospheres of Jupiter and Saturn. *Journal of Geophysical Research*, *116*, A05209. https://doi.org/10.1029/2010JA016294

Bunce, E. J., Cowley, S. W. H., Alexeev, I. I., Arridge, C. S., Dougherty, M. K., Nichols, J. D., & Russell, C. T. (2007). Cassini observations of the variation of Saturn's ring current parameters with system size. *Journal of Geophysical Research*, *112*, A10202. https://doi.org/10.1029/2007JA012275

Connerney, J. E. P., Acuña, M. H., & Ness, N. F. (1981). Modeling the Jovian current sheet and inner magnetosphere. *Journal of Geophysical Research*, *86*(A10), 8370–8384. https://doi.org/10.1029/JA086iA10p08370

Connerney, J. E. P., Acuña, M. H., & Ness, N. F. (1983). Currents in Saturn's magnetosphere. *Journal of Geophysical Research*, *88*(A11), 8779–8789. https://doi.org/10.1029/JA088iA11p08779

Dougherty, M. K., Khurana, K. K., Neubauer, F. M., Russell, C. T., Saur, J., Leisner, J. S., & Burton, M. E. (2006). Identification of a dynamic atmosphere at Enceladus with the Cassini magnetometer. *Science*, *311*, 1406–1409. https://doi.org/10.1126/science.1120985

Escoubet, C. P., Taylor, M. G. G. T., Masson, A., Laakso, H., Volpp, J., Hapgood, M., & Goldstein, M. L. (2013). Dynamical processes in space: Cluster results. *Annales Geophysicae*, *31*, 1045–1059. https://doi.org/10.5194/angeo-31-1045-2013

Hardy, F., Achilleos, N., & Guio, P. (2019). A self-regulating equilibrium magnetopause model with applications to Saturn. *Journal of Geophysical Research: Space Physics*, *124*, 6833–6849. https://doi.org/10.1029/2019JA026751

Jia, Y. D., Russell, C. T., Khurana, K. K., Ma, Y. J., Najib, D., & Gombosi, T. I. (2010). Interaction of Saturn's magnetosphere and its moons: 2. Shape of the Enceladus plume. *Journal of Geophysical Research*, *115*, A04215. https://doi.org/10.1029/2009JA014873

Kanani, S. J., Arridge, C. S., Jones, G. H., Fazakerley, A. N., McAndrews, H. J., Sergis, N., et al. (2010). A new form of Saturn's magnetopause using a dynamic pressure balance model, based on in situ, multi-instrument Cassini measurements. *Journal of Geophysical Research*, *115*, A06207. https://doi.org/10.1029/2009JA014262

Kaufmann, R. L., & Konradi, A. (1969). Explorer 12 magnetopause observations: Large-scale nonuniform motion. *Journal of Geophysical Research*, *74*(14), 3609–3627. https://doi.org/10.1029/JA074i014p03609

Kellett, S., Arridge, C. S., Bunce, E. J., Coates, A. J., Cowley, S. W. H., Dougherty, M. K., et al. (2010). Nature of the ring current in Saturn's dayside magnetosphere. *Journal of Geophysical Research*, *115*, A08201. https://doi.org/10.1029/2009JA015146

Khurana, K. K., Dougherty, M. K., Russell, C. T., & Leisner, J. S. (2007). Mass loading of Saturn's magnetosphere near Enceladus. *Journal of Geophysical Research*, *112*, A08203. https://doi.org/10.1029/2006JA012110

Masters, A., Mitchell, D. G., Coates, A. J., & Dougherty, M. K. (2011). Saturn's low-latitude boundary layer: 1. Properties and variability. *Journal of Geophysical Research*, *116*, A06210. https://doi.org/10.1029/2010JA016421

Petrinec, S. M., & Russell, C. T. (1997). Hydrodynamic and MHD equations across the bow shock and along the surfaces of planetary obstacles. *Space Science Reviews*, *79*(3/4), 757–791. https://doi.org/10.1023/A:1004938724300

Pilkington, N. M., Achilleos, N., Arridge, C. S., Guio, P., Masters, A., Ray, L. C., et al. (2015). Internally driven large-scale changes in the size of Saturn's magnetosphere. *Journal of Geophysical Research A: Space Physics*, *120*, 7289–7306. https://doi.org/10.1002/2015JA021290

Pilkington, N. M., Achilleos, N., Arridge, C. S., Masters, A., Sergis, N., Coates, A. J., & Dougherty, M. K. (2014). Polar confinement of Saturn's magnetosphere revealed by in situ Cassini observations. *Journal of Geophysical Research: Space Physics*, *119*, 2858–2875. https://doi.org/10.1002/2014JA019774

Sergis, N., Krimigis, S. M., Roelof, E. C., Arridge, C. S., Rymer, A. M., Mitchell, D. G., et al. (2010). Particle pressure, inertial force, and ring current density profiles in the magnetosphere of Saturn, based on Cassini measurements. *Geophysical Research Letters*, *37*, L02102. https://doi.org/10.1029/2009GL041920

Shue, J.-H., Chao, J. K., Fu, H. C., Russell, C. T., Song, P., Khurana, K. K., & Singer, H. J. (1997). A new functional form to study the solar wind control of the magnetopause size and shape. *Journal of Geophysical Research*, *102*, 9497–9512. https://doi.org/10.1029/97JA00196

Slavin, J. A., Smith, E. J., Spreiter, J. R., & Stahara, S. S. (1985). Solar wind flow about the outer planets: Gas dynamic modeling of the Jupiter and Saturn bow shocks. *Journal of Geophysical Research*, *90*, 6275–6286. https://doi.org/10.1029/JA090ia07p06275

Sorba, A. M., Achilleos, N. A., Guio, P., Arridge, C. S., Pilkington, N. M., Masters, A., et al. (2017). Modeling the compressibility of Saturn's magnetosphere in response to internal and external influences. *Journal of Geophysical Research: Space Physics*, *122*, 1572–1589. https://doi.org/10.1002/2016JA023544

Tokar, R. L., Johnson, R. E., Hill, T. W., Pontius, D. H., Kurth, W. S., Crary, F. J., et al. (2006). The interaction of the atmosphere of Enceladus with Saturn's plasma. *Science*, *311*, 1409–1412. https://doi.org/10.1126/science.1121061

Tsyganenko, N. A. (1998). Modeling of twisted/warped magnetospheric configurations using the general deformation method. *Journal of Geophysical Research*, *103*(A10), 23,551–23,563. https://doi.org/10.1029/98JA02292